Electroexcitation of the $T_0 + 1$ giant $M1$ resonance in ^{58,60}Ni

R. A. Lindgren,* W. L. Bendel, E. C. Jones, Jr., L. W. Fagg, and X. K. Maruyama†
Naval Research Laboratory, Washington, D. C. 20375

J. W. Lightbody, Jr. and S. P. Fivozinsky
National Bureau of Standards, Gaithersburg, Maryland 20234

(Received 24 April 1975; revised manuscript received 18 May 1976)

Using inelastic electron scattering, several isobaric analog 1^+ states between 9 and 13 MeV excitation in ^{58}Ni and ^{60}Ni have been found. They are identified as components of the $T_0 + 1$ giant $M1$ state in ^{58,60}Ni.

[NUCLEAR REACTIONS ^{58}Ni(e,e'), $E = 40$, 50, 60, and 75 MeV; measured $\sigma(E, 163°)$; ^{58,60}Ni(e,e'), $E = 40$, 50, and 60 MeV; measured $\sigma(E, 180°)$; measured $B(M1)\uparrow$; deduced J^π; enriched targets.]

I. INTRODUCTION

The particle-hole model, which has been so successful in accounting for the features of the well known giant $E1$ resonance, predicts[1,2] the existence of "spin-flip" giant $M1$ states of the general form $[(l_{j>})^{-1}(l_{j<})]$ as a systematic feature of nuclei. The $M1$ strength is predicted to be strongest in nuclei where l is large and where the lower partner of a spin-orbit pair is a closed shell. Thus far, strong $M1$ transitions have been found in light nuclei[3] ($A < 40$) involving low-l orbits and near $A \sim 140$[4] and ^{208}Pb.[5,6] In the nickel nuclei, strong $M1$ transitions to $T_0 + 1$, 1p-1h states of the form $[f_{7/2}^{-1} f_{5/2}]_{1^+}$ are expected based on simple model calculations[7] and inferences from results of charge-exchange experiments,[7,8] but no direct excitation or measurement of the strength has been made. In fact no identification of the $T_0 + 1$ giant $M1$ state(s) in any neutron excess even-even nucleus has been reported. The purpose of this work, therefore, is to locate the $T_0 + 1$ and T_0 giant $M1$ strength in ^{58,60}Ni.

The $M1$ strengths are also of interest because the matrix elements can be related to those in processes such as radiative-pion production,[9] β-decay,[10] charge-exchange reactions,[7,8] and inelastic proton scattering.[11] Consequently, knowledge of the $M1$ strength is important and useful in connecting those processes whose matrix elements primarily depend on the nucleon intrinsic spin.

II. EXPERIMENT

The experiment was performed using backward-angle inelastic electron scattering at low momentum transfer, which is a known technique[3] to systematically excite $M1$ states. We have made measurements at incident electron energies of 40.5, 50.5, and 61.3 MeV on enriched targets (> 99%) or ^{58,60}Ni using the 180° electron scattering system[3] at the Naval Research Laboratory and have made measurements at incident energies 40.2, 49.5, 60.0, and 75.1 MeV at $\theta = 163°$ on ^{58}Ni using the National Bureau of Standards electron scattering facility.[12] Electrons were detected in an array of detectors mounted in the focal plane of a magnetic spectrograph. Data were stored on magnetic tape and replayed for analysis. Data were taken at the two different back angles on ^{58}Ni to be sure the measured cross sections were consistent with a pure transverse multipole, most probably a magnetic multipole. Since the data taken at NBS at $\theta = 163°$ were obtained with higher energy resolution and less ambiguous background, they were used to compare with model calculations to deduce the magnetic dipole transition strength in ^{58}Ni. For ^{60}Ni the 180° data were used to deduce the transition strength, since no ^{60}Ni data were taken at $\theta = 163°$. Absolute cross sections were obtained by making measurements relative to the ^{12}C ground state and/or 15.1 MeV, $M1$ state.

III. EXPERIMENTAL RESULTS

A. ^{58}Ni

A portion of a spectrum from ^{58}Ni bombarded by 40 MeV electrons is shown in Fig. 1 taken at NBS at $\theta = 163°$ and at NRL at $\theta = 180°$. The comparison shows that at both angles, states are observed at 9.85, 10.15, 10.55, 10.65, and 11.05 MeV excitation. With the background chosen as in Fig. 1 the cross sections of the aforementioned levels are the same at 180° and 163° to within approximately 20%. Based on the known angular dependence of

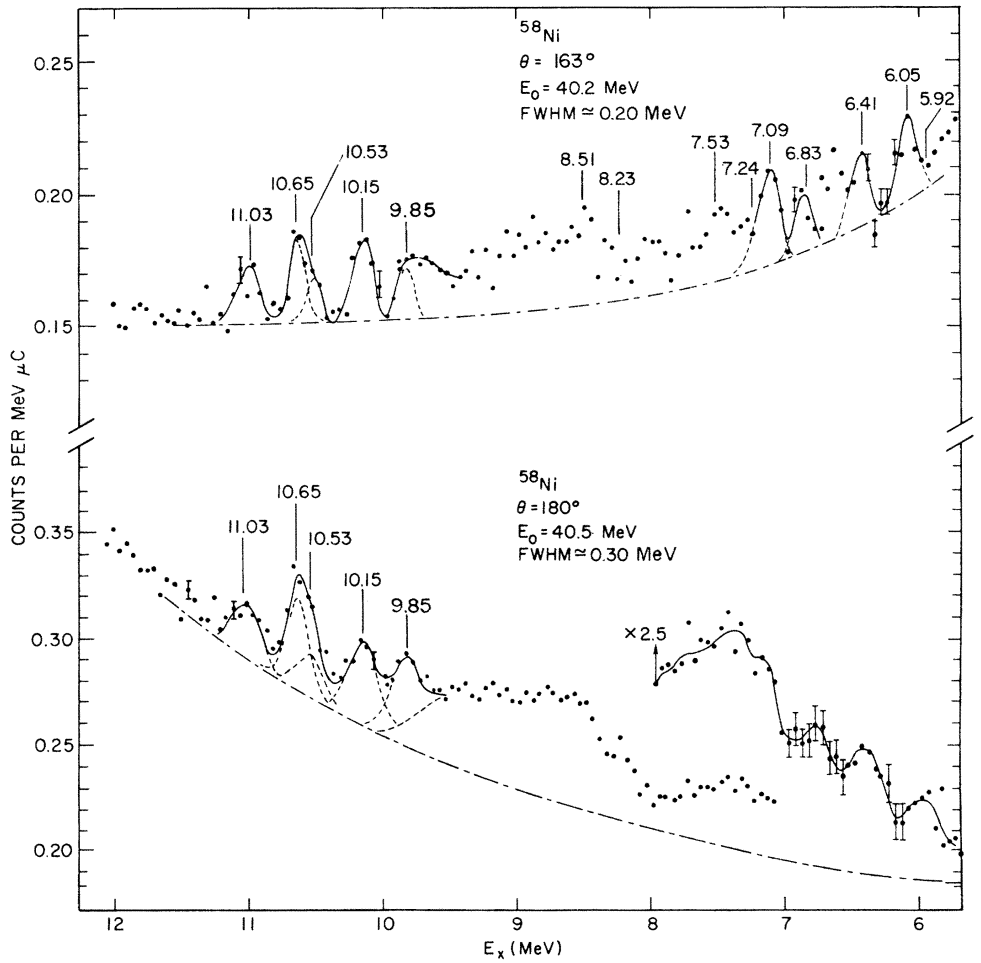

FIG. 1. Spectra observed at $\theta = 163°$ and $\theta = 180°$ from 40 MeV electrons incident on an enriched ^{58}Ni target. The dashed lines represent curve fitted peaks and the dot-dash line is the elastic radiation tail plus background. The two curves added together give the full lines through the data points.

the electron scattering cross section,[13] this near equality implies that the states under consideration are predominantly excited by a transverse process and not a longitudinal one. This conclusion is strongly dependent on how the background was drawn, unfortunately not a unique choice. However, in each of the spectra, it was not possible to make this choice consistent with the cross sections having a significant longitudinal component. We may conclude that the excitation processes involve only nuclear magnetization currents if no longitudinal components are observed.

At $\theta = 163°$ the dot-dash line in Fig. 1 is the result of a radiation tail calculation[14] normalized to fit the low excitation energy part of the spectrum ($E_x < 3.0$ MeV). Because of the difficulty in calculating or measuring the background at $\theta = 180°$ including radiation tails, the dot-dash line was estimated in the 180° spectrum in Fig. 1. The level cross sections were then obtained by fitting the peaks with a line shape that is the same as the elastic peak.

The increasing background and the higher density of states excited below $E_x = 10$ MeV in Fig. 1 make it more difficult to identify states in the range $10.0 \geq E_x \geq 5.5$ MeV. However, by comparing the spectrum at $\theta = 163°$ at 40 MeV in Fig. 1 with spectra at 50, 60, and 75 MeV, some information on the cross sections at 40 MeV can be obtained. This is because at the higher bombarding energies some of the lower excited states are more easily identified and, therefore, can be used to help locate the state in the 40 MeV spectrum. Spectra of electrons are shown in Figs. 2 and 3 for bombarding energies $E_0 = 60$ and 75.1 MeV, respectively. In Fig. 2 spectra taken at $\theta = 163°$ and $\theta = 180°$ at similar incident

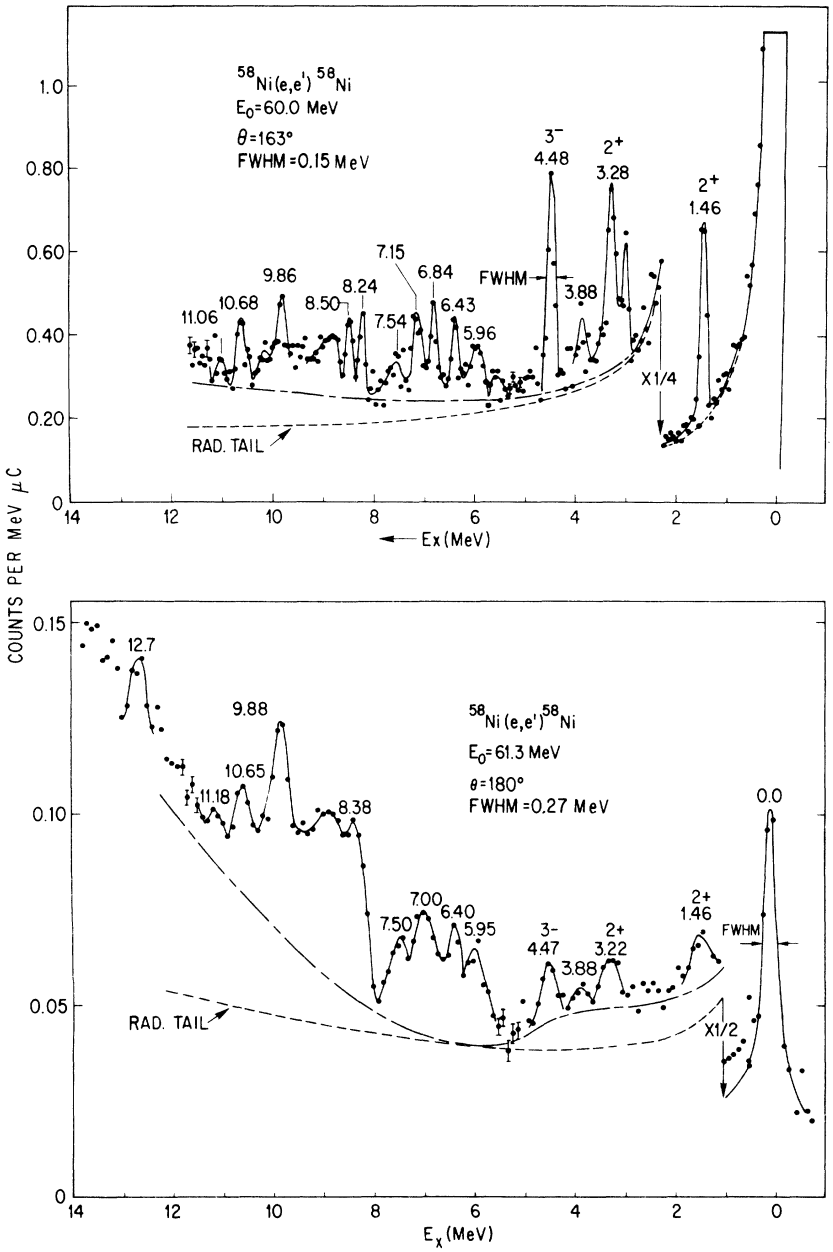

FIG. 2. Spectra observed at $\theta = 163°$ from 60.0 MeV electrons and at $\theta = 180°$ from 61.3 MeV electrons incident on ^{58}Ni. The lines through the data points are to guide the eye.

electron energies are compared. The lines drawn through the data points are to guide the eye. A number of states in the range $7.85 \geq E_x \geq 5.50$ MeV can be seen at both angles. These states also persist at 75.1 MeV as is shown in Fig. 3. The first $J^\pi = 2^+$ and 3^- states in ^{58}Ni are identified at $E_x = 1.46$ and 4.48 MeV in Figs. 2 and 3 as well as a known 2^+ state at 3.26 MeV. The 1.46, 3.26, and 4.48 MeV states are known states excited strongly by longitudinal $E2$ and $E3$ transitions and were previously observed by Duguay *et al.*[15] The excitation strength of the states in the range $7.85 \geq E_x \geq 5.50$ do not have the same angular dependence as the 1.46, 3.26, or 4.48 MeV states, as can be observed by comparing their relative cross sections at $\theta = 163°$ and $\theta = 180°$ in Fig. 2. A more quantitative discussion on these states is presented in the next section.

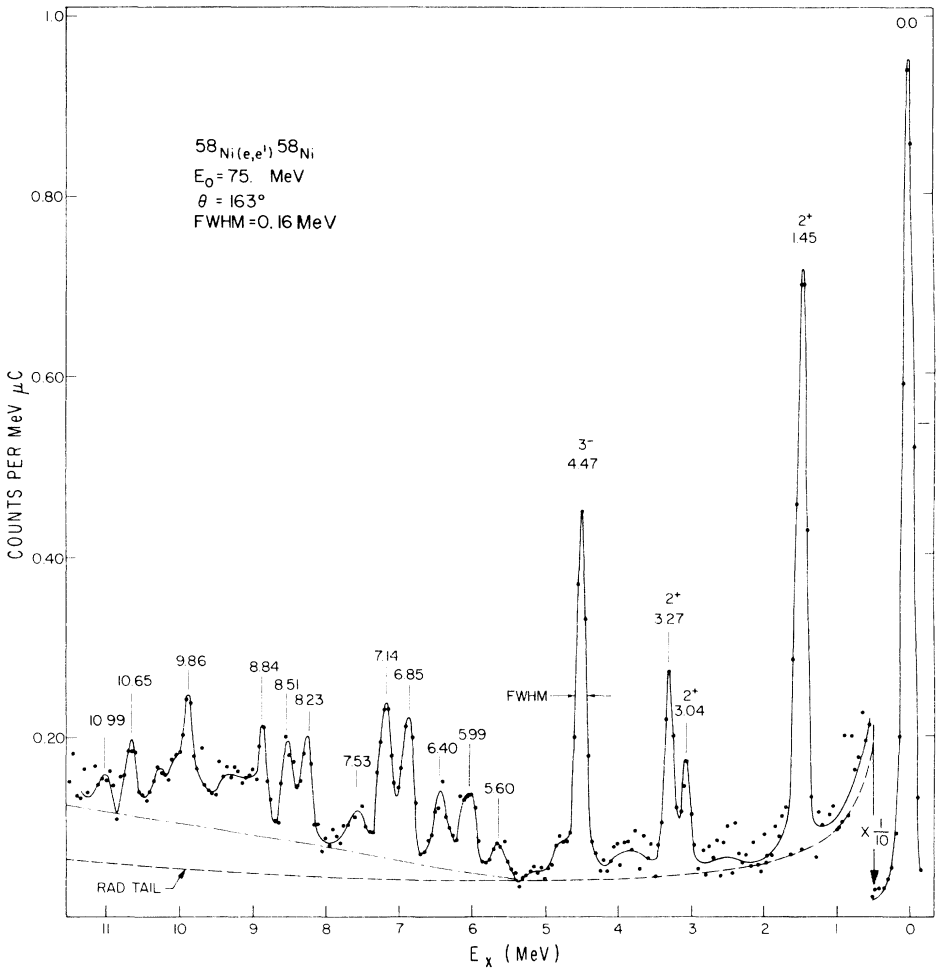

FIG. 3. Spectrum observed at $\theta = 163°$ from 75.1 MeV electrons incident on ^{58}Ni. The lines through the data points are to guide the eye.

Expanded portions of the observed spectra at $\theta = 163°$ for bombarding energies 49.5, 60.0, and 75.1 MeV are shown in Fig. 4. The dashed lines are curve fitted to the data using a line shape with the same shape as the elastic scattering peak. The area under a peak defined by a dashed line is the measured cross section. Most all of the excited states in the range $11.0 \geq E_x \geq 5.5$ are observed at all three incident energies shown in Fig. 4.

The dot-dash line drawn in Figs. 2, 3, and 4 is an estimate of the background determined in the following way. The results from the radiative tail calculation[14] fitted the data at excitation energies $E_x \leq 3.0$ MeV, but failed at $E_x \geq 5.0$ MeV (see Figs. 2 and 3). We therefore, adjusted our estimate of the background at the higher excitation energies until it smoothly fit onto the radiative tail calculation below 3.0 MeV. In addition in order to fit the background in the range $E_x \leq 3.0$ MeV, the radiative tail calculated cross sections had to be uniformly increased by about 30%.

A tabulation of the cross sections and average energies for states observed at $\theta = 163°$ is shown in Table I. The energy for each state is obtained by averaging the values obtained from the various spectra. The uncertainty on the cross sections is generally ± (20–30)% and is determined by (i) the uncertainty in choosing the background plus radiation tail, and (ii) the influence of neighboring partially resolved levels. We realize that our method for determining the background is somewhat subjective, and a different choice may give rise to absolute cross sections that differ from the present values by more than the given uncertainty. However, we have used a consistent procedure as described to choose the background for the different

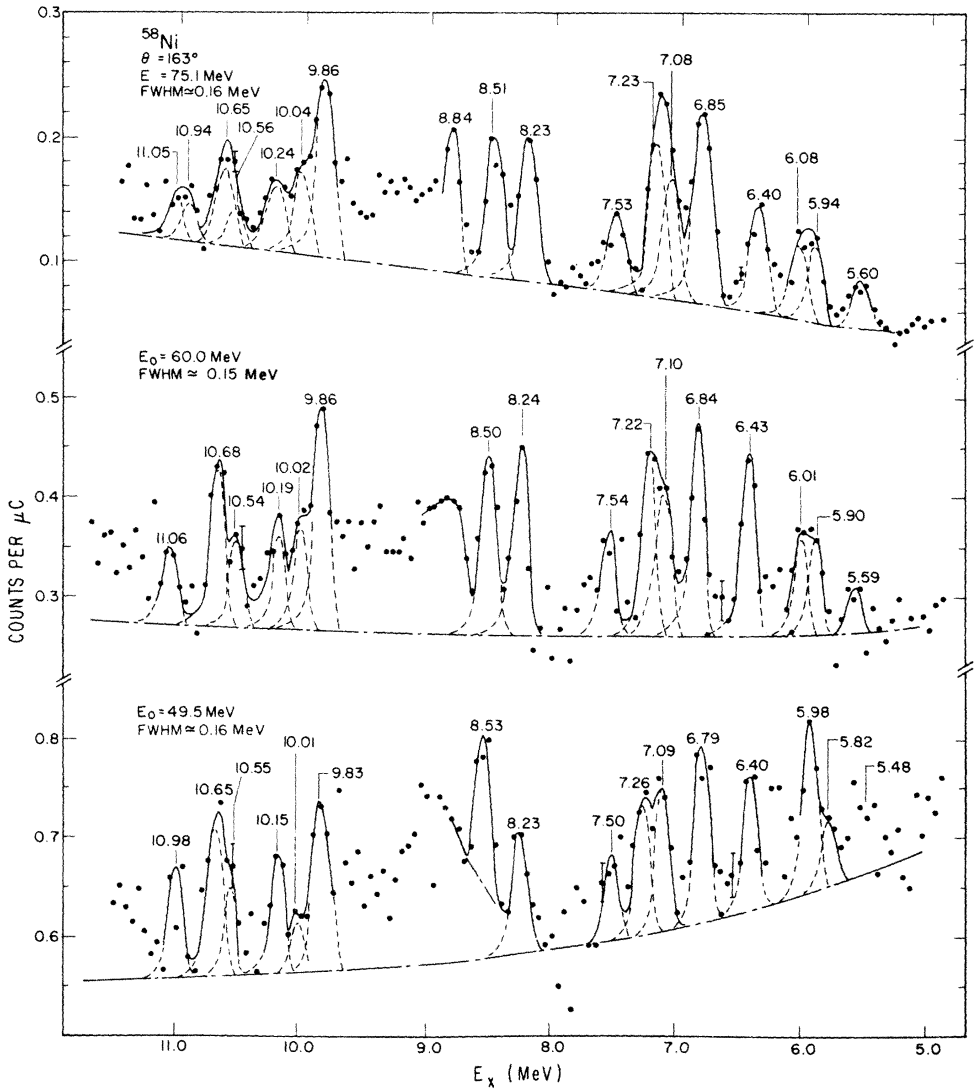

FIG. 4. Expanded portions of spectra observed at $\theta = 163°$ from 49.5, 60.0, and 75.1 MeV electrons incident on ^{58}Ni. The dashed lines represent curve fitted peaks and the dot-dash line is the elastic radiation tail plus background. The two curves added together give the full lines through the data points.

spectra and within this procedure the tabulated uncertainties apply.

B. ^{60}Ni

A limited amount of data have been taken on ^{60}Ni at $\theta = 180°$ at incident electron energies of 40.5 and 50.5 MeV. A portion of the spectrum at 40.5 and 50.5 MeV is shown in Fig. 5. States are observed at 11.9 and 12.3 MeV and are also tabulated in Table II. The measured cross section in units of nb/sr for the 11.9 and 12.3 MeV states are 9.7± 2.4 and 4.9± 1.2 at 40.5 MeV incident electron energy and 5.4± 1.3 and 1.6± 0.6, respectively, at 50.5 MeV.

IV. DISCUSSION OF EXPERIMENTAL RESULTS

A. $M1$ transitions to $T = T_0 + 1, J^\pi = 1^+$ states in ^{58}Ni

1. Comparison with predictions from the known analog states in ^{58}Co

The states excited at the energies 9.85, 10.18, 10.55, 10.66, and 11.03 MeV are candidates for $T = T_0 + 1, J^\pi = 1^+$ states or isobaric analog states in ^{58}Ni. These states would have as their parent analogs low lying 1^+ states in ^{58}Co. The lowest five 1^+ states in ^{58}Co are the 1.05, 1.43, 1.73, 1.86, and 2.24 MeV states.[16] Adding to these energies the Coulomb energy difference[17] between

TABLE I. Averaged measured excitation energies and differential cross sections at $\theta = 163°$ at four incident electron bombarding energies for levels in ^{58}Ni.

E_x (MeV) (Ave)	$d\sigma/d\Omega$ (nb/sr) E_0 (MeV) 40.2	49.5	60.0	75.1
1.46		58.5 ± 14.6	41.8 ± 2.9	21.1 ± 4.4
4.46		9.4 ± 2.0	13.6 ± 1.3	12.3 ± 0.6
5.92, 6.05	10.2 ± 2.6	5.4 ± 0.6	4.8 ± 0.5	3.7 ± 0.5
6.41	7.9 ± 1.8	4.5 ± 0.6	4.5 ± 0.5	2.5 ± 0.5
6.83	7.1 ± 1.8	6.1 ± 0.8	5.4 ± 0.5	4.7 ± 0.5
7.09, 7.24	13.4 ± 2.2	9.3 ± 0.8	8.0 ± 0.7	6.7 ± 0.7
7.53		3.7 ± 0.6	2.7 ± 0.6	2.0 ± 0.4
8.23	≤4.8	4.3 ± 0.6	4.9 ± 0.5	3.5 ± 0.5
8.51		6.5 ± 1.7 [a]	4.7 ± 0.4	3.5 ± 0.5
9.85	(8.1) [b]	5.6 ± 0.7	6.0 ± 0.5	4.3 ± 0.5
10.18	14.9 ± 1.5	4.0 ± 0.9	2.4 ± 0.5	1.4 ± 0.5
10.55, 10.66	15.7 ± 1.5	8.3 ± 1.0	6.2 ± 0.9	2.9 ± 1.2
11.03	9.1 ± 1.0	4.0 ± 0.7	2.2 ± 0.6	$0.9 \leq d\sigma/d\Omega \leq 1.9$ [c]

[a] Two background extremes were chosen and then averaged to get the peak cross section (see Fig. 4).

[b] Estimated cross section (see Fig. 1).

[c] The upper limit is the sum of the two possible peaks and the lower limit is just one of them (see Fig. 4).

^{58}Ni-^{58}Co, 9.218 MeV, and the total ground state mass energy difference, 0.388 MeV, and subtracting the neutron-proton mass difference, 0.782 MeV, the predicted positions of the analog states in ^{58}Ni occur at 9.87, 10.25, 10.55, 10.68, and 11.06 MeV. These energies lie fairly close to the measured ones, which suggest they may indeed be the corresponding analog states.

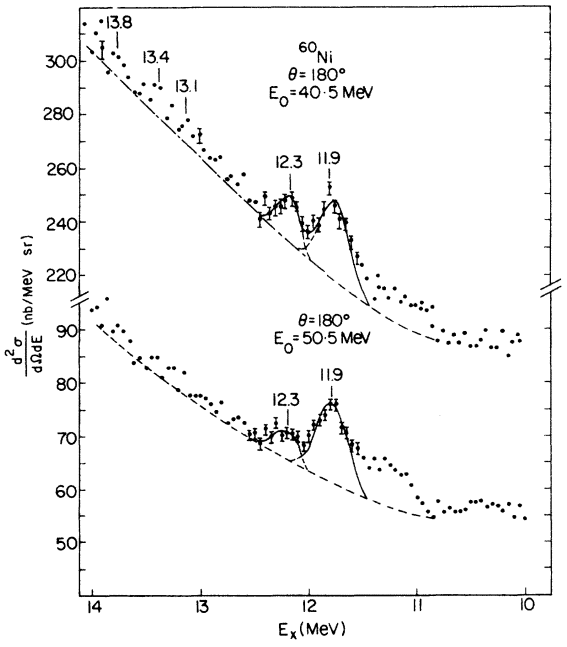

FIG. 5. Portion of spectrum observed at $\theta = 180°$ from 40.5 and 50.5 MeV electrons incident on a ^{60}Ni target.

TABLE II. Measured excitation energies, J^π assignments, and reduced $M1$ transition probabilities for levels in ^{58,60}Ni.

E_x (MeV) Exp [a]	J^π	E_x (MeV) Predicted [b]	Parent	$B(M1)\downarrow$ (μ_N^2) [c]	$\Gamma(M1)$ (eV) [d]
^{58}Ni		^{58}Ni	^{58}Co		
9.85	(1^+)	9.87	1.05	(0.32) [e]	(3.4) [e]
10.18	1^+	10.25	1.43	0.59	7.2
10.55	1^+	10.55	1.73	0.21	3.0
10.66	1^+	10.68	1.86	0.41	5.7
11.03	1^+	11.06	2.24	0.36	5.6
^{60}Ni		^{60}Ni	^{60}Co		
11.9	1^+	11.87	0.74	0.46	8.9
12.3	1^+	12.34	1.21	0.26	5.6
13.1	(1^+)	13.11	1.98	≤0.06	≤1.5
13.4	(1^+)	13.35	2.22	≤0.06	≤1.6
13.8	(1^+)	13.84	2.71	≤0.06	≤1.8

[a] Energy uncertainty is ±0.04 MeV in ^{58}Ni and ±0.1 MeV in ^{60}Ni.

[b] To get predicted energy in ^{58}Ni add 8.82 MeV to excitation energies in ^{58}Co and for ^{60}Ni add 11.13 MeV.

[c] $M1$ strength uncertainty is estimated to be about ±25% for individual levels.

[d] $\Gamma(M1) = 0.0115\, E_x^3\, B(M1)$.

[e] Tentative $M1$ identification (see text).

2. *M1 cross section predictions from distorted wave Born approximations calculations*

In order to determine the multipolarity of these transitions independent of the analog systematics, we have compared the measured dependence of the inelastic electron scattering cross section on the bombarding energy to distorted wave Born approximation (DWBA) predictions. The DWBA calculations were done with the computer code DUELS using parameters describing the nuclear charge and radius from previous electron scattering ^{58}Ni experiments.[15] The transition density is calculated from the computer code MICRODENS, which has been described in detail elsewhere.[18] The transition density calculations, depending on the multipolarity, include the longitudinal or electric static charge density and the transverse convection and magnetization current densities. The convection current arises from the effects of orbital motion of the nucleons and magnetization current arises from the effects of the nucleon intrinsic spin or magnetic moment. It is the latter term which is dominant in the case of spin-flip magnetic dipole transitions. This is illustrated in Fig. 6 where the spin and current components of the transition density are plotted for comparison. The MICRODENS program calculates the transition density in j-j coupling from shell model wave functions based on an oscillator potential well. If the shell model wave functions, or equivalently, the one-body density matrix elements are known, then MICRODENS can be used to calculate the appropriate multipole transition density, which is then used as input to DUELS.

In the nickel mass region neither a complete nor a truncated fp shell model calculation has been made for the $T = T_0 + 1$, $J^\pi = 1^+$ states. In the fp space, matrix elements of the $M1$ operator between any combination of the orbits $f_{7/2}$, $f_{5/2}$, $p_{3/2}$, and $p_{1/2}$ will contribute, in general, to the $M1$ transition strength including the diagonal terms. However, the cross section deduced from the isovector $M1$ matrix elements between the orbits $(f_{7/2}f_{5/2})$, $(f_{7/2}f_{7/2})$, and $(p_{3/2}p_{1/2})$ is 20–100 times stronger than the orbits $(f_{5/2}f_{5/2})$, $(p_{1/2}p_{1/2})$, and $(p_{3/2}f_{5/2})$ at low q ($q \leq 190$ MeV/c corresponding to $E_0 \leq 50$ MeV and $E_x \simeq 10$ MeV). Furthermore, in the limit of the extreme single particle model where ^{56}Ni is considered a closed core, the $f_{7/2}$ orbit is completely filled and the $f_{5/2}$ orbit is empty. Therefore, it is expected that the main component of the $T = T_0 + 1$, $J^\pi = 1^+$ state(s) will be the spin-flip $(f_{7/2}^{-1}f_{5/2})$ particle-hole configuration. In any case the ratio of the cross section to the reduced $M1$ transition probability is about constant for the $\Delta l = 0$ isovector $M1$ matrix elements in the fp shell at low q and, therefore, the extracted $M1$ strength is independent of the orbital admixtures considered to within 5%–10%. The main effect of not considering the weaker admixed particle-hole configurations will be discrepancies in fitting the data at high q ($q \geq 110$ MeV/c corresponding to $E_0 \geq 60$, $E_x = 10$ MeV) where the $(f_{7/2}^{-1}f_{5/2})$ configuration has a minimum in the form factor (see Fig. 7). This will have little bearing on our ability to assign the spin and extract the $M1$ strength at low q.

It is noted that the $(p_{3/2}^{-1}f_{5/2})$ configuration gives rise to a $\Delta l = 2$ forbidden $M1$ transition and does not contribute to the reduced $M1$ transition strength at the photon point. This configuration yields a cross section that is more than 100 times weaker than the $(f_{7/2}^{-1}f_{5/2})$ at our bombarding energies and is, therefore, expected to be negligible.

3. *Comparison of* DWBA *predictions with experiment*

Figure 7 shows a comparison of the data to calculated fits for various multipoles. For the $M3$, $E2$, and $M1$ transitions the wave function of the particle-hole state was assumed to be of the form $1/\sqrt{2}\,[(f_{7/2}^{-1}f_{5/2})_p - (f_{7/2}^{-1}f_{5/2})_n]$. For the $E1$ and $M2$ transitions an analogous form was assumed with the $f_{5/2}$ orbit replaced by $g_{9/2}$. In Fig. 7 the trend of the $M1$ cross section predictions from 40

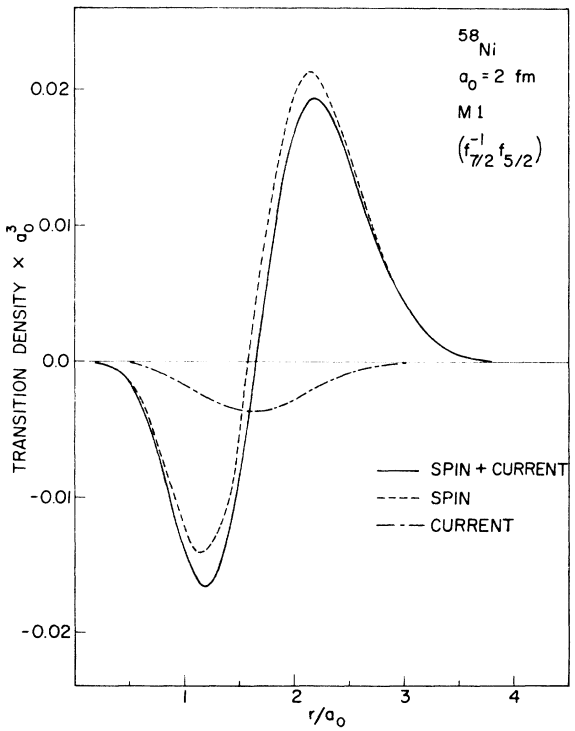

FIG. 6. Plot of the spin and current components of the transition density for ^{58}Ni assuming an $M1$ transition from an $(f_{7/2}^{-1}f_{5/2})$ particle-hole configuration.

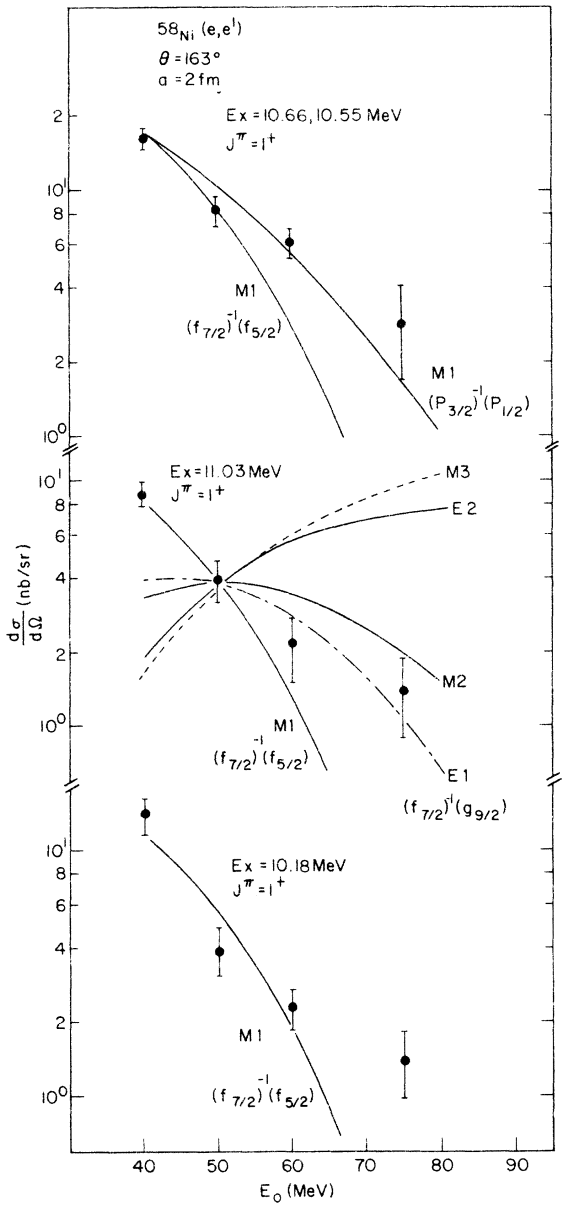

FIG. 7. Comparison of measured cross section with DWBA predictions plotted as a function of E_0 for states $E_x \geq 10$ MeV.

to 50 MeV is similar whether a $f_{7/2}^{-1}f_{5/2}$ or $p_{3/2}^{-1}p_{1/2}$ configuration is assumed. An oscillator constant of $a = 2.0$ fm was used. Variations from 1.8 to 2.2 fm did not significantly alter the shapes of the curves in Fig. 7. The best fit to the data in Fig. 7 in the practically model-independent region below 50 MeV is the $M1$ assignment. At $E_0 = 60$ to 75 MeV, where the momentum transfer q corresponds roughly to the diffraction minimum of the form factor, larger discrepancies are expected.

Since the extraction of the $M1$ strength is less model dependent as one goes towards lower q, the reduced $M1$ transition probability in nuclear magnetons squared (μ_N^2) for each state is obtained by normalizing the calculated cross section based on the $f_{7/2}^{-1}f_{5/2}$ configuration to the measured one at $E_0 = 40$ MeV. The ^{58}Ni results are shown in Table II. The DWBA calculations together with the analog systematics imply that the 10.18, 10.55, 10.66, and 11.03 MeV states in ^{58}Ni have $T = 2$, $J^\pi = 1^+$. In Table II the $M1$ strength is tabulated in nuclear square magnetons (μ_N^2) and in electron volts (eV). The reduced $B(M1)\uparrow$ strengths range from about 0.2 to $0.6\mu_N^2$ and sum to about $1.9\mu_N^2$ for ^{58}Ni. The $M1$ strength is spread over about five levels within an energy interval of about 1 MeV. The centroid of the $M1$ strength is about 10.5 MeV excitation, not far from 9.5 MeV excitation, the predicted[7] position by a simple shell model particle-hole calculation based on the $f_{7/2}$ and $f_{5/2}$ orbits.

Our identification of the $M1$ states is partly consistent with that of Flynn and Garrett who inferred from the charge-exchange (t, ^{3}He) reaction[8] that the parent analogs of the giant $M1$ in ^{58}Ni are the 1.05 and 1.86 MeV states in ^{58}Co, which would be the 9.85 and 10.66 MeV states in ^{58}Ni. The behavior of the cross section of the 9.85 MeV state is shown in Fig. 8. Because of the nature of the spectrum between 8.5 and 9.8 MeV excitation, the background under the 9.85 MeV peak is quite uncertain. When the cross section is assumed to be that due to the area under the dashed curve shown for this state in Fig. 1, then there is a decrease in cross section from 40 to 50 MeV, indicating the presence of an $M1$ transition. From 50 to 75 MeV its behavior is more similar to an $M2$ transition. Consequently, it appears that two levels may be excited. Further support for the $M1$ transition is the point that it might be surprising that the first analog 1^+ state is not excited at all, since the next four analog 1^+ states are systematically excited at $E_0 = 40$ MeV.

B. $M1$ transitions in $T_0 + 1$, $J^\pi = 1^+$ states in ^{60}Ni

At $\theta = 180°$ definite states were observed at $E_x = 11.9$ and 12.3 MeV in ^{60}Ni. The predicted positions of the analog levels in ^{60}Ni based on the first five known[19] $J^\pi = 1^+$ states in ^{60}Co are at $E_x = 11.87$, 12.34, 13.11, 13.35, and 13.84 MeV. These energies were obtained in an analogous way to ^{58}Ni. The 11.9 and 12.3 MeV levels are in agreement with the predicted positions of the 1^+ analog levels. The decrease in cross section of both levels from 40.5 and 50.5 incident electron energy is about a factor of 2 and 3, respectively, with about a 30% uncertainty. By normalizing the calculated $M1$ cross section to the measured cross section at $E_0 = 40.5$ MeV and $\theta = 180°$ using the same model as

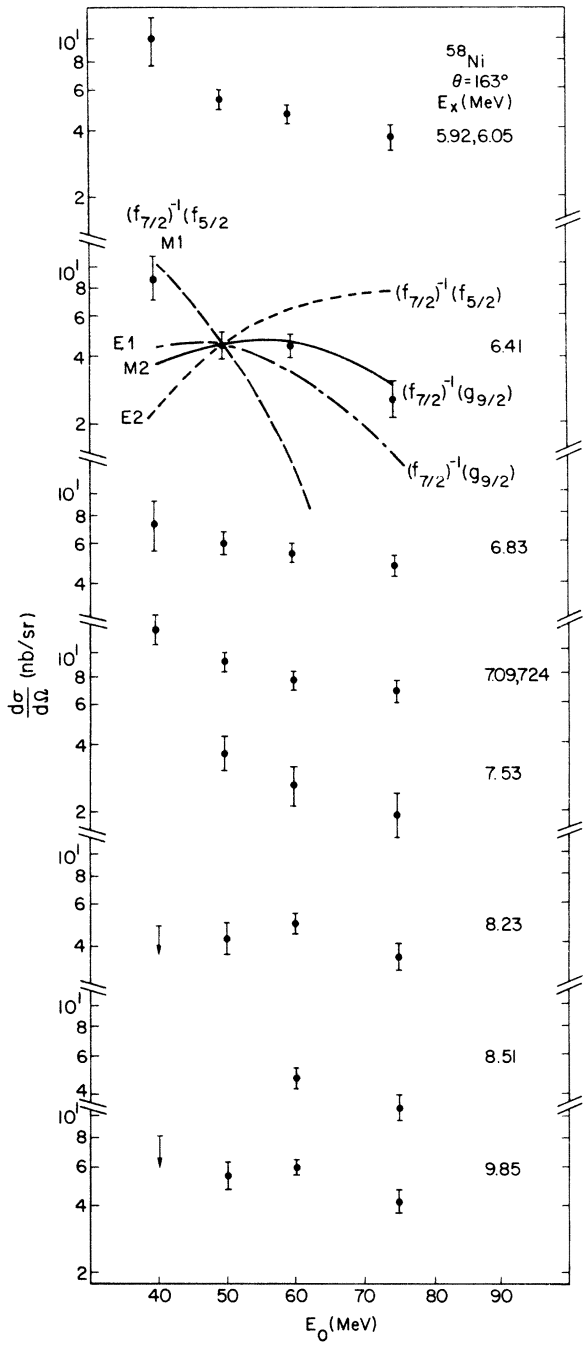

FIG. 8. Comparison of measured cross section with DWBA predictions plotted as a function of E_0 for states in the range $9.8 \geq E_x \geq 5.50$ MeV.

in ^{58}Ni, the reduced $M1$ transition strength was obtained. The results are summarized in Table II together with ^{58}Ni. In ^{60}Ni the maximum $M1$ strength sums to $0.90\mu_N^2$, about half the value in ^{58}Ni. The centroid of the strength lies at about 12.1 MeV excitation, 1.6 MeV higher than in ^{58}Ni.

C. $T_0 \rightarrow T_0$, $M1$ and $M2$ transitions to states in the range $10.0 \geq E_x \geq 5.5$ MeV in ^{58}Ni

A number of excited states have been observed below 10 MeV excitation in ^{58}Ni. It might be expected that some of these states would have $T_0 = 1$, $J^\pi = 1^+$ assignments, which would correspond to the lower isospin counterpart of the giant $M1$ strength observed in the states above 10 MeV.

A comparison of spectra between $\theta = 163°$ and $\theta = 180°$ near $E_0 = 60$ MeV shown in Fig. 2 reveals that the dominant excitation mode for states in the range $7.85 \geq E_x \geq 5.50$ MeV is transverse. The cross section summed over this range yields a value that is 1.3 ± 0.2 times larger at $\theta = 163°$ than at $\theta = 180°$. Using a longitudinal (charge) transition density derived from a two parameter Fermi distribution[15] with the transverse current contribution given by Siegert's theorem,[20] the cross section for excitation of a state at $E_x = 7$ MeV is 4 times larger at $\theta = 163°$ than at 180°. Since the ratio for a pure transverse mode of excitation would be about 1.1, we conclude that the states are predominantly excited by the transverse mode. Note that the measured cross section ratio from 163° to 180° for the known longitudinal $E2$ and $E3$ transitions to states at 1.46 and 4.46 MeV, respectively, is about 20 to 1 and 5 to 1, respectively. This is what is expected based on the known charge distributions. Our measured cross sections from $E_0 = 40$ to 75 MeV at $\theta = 163°$ for the $E_x = 1.46$ and 4.46 MeV states also agree within 20% of the values measured by Duguay *et al.*[15]

The cross section for discernible states in the range $10.0 \geq E_x \geq 5.5$ MeV is plotted in Fig. 8 as a function of E_0. Within the limits of the error bars these distributions are very similar, particularly from 50 to 75 MeV. A comparison of the calculated transverse $E1$, $E2$, $M1$, and $M2$ transitions are shown fit to the 6.41 MeV level, which is representative of the data in Fig. 8. The $E1$ and $M2$ transitions were calculated from a particle-hole wave function of the form $1/\sqrt{2}\,[(f_{7/2}^{-1}g_{9/2})_p + (f_{7/2}^{-1}g_{9/2})_n]$. The $(f_{7/2}^{-1}g_{7/2})$, $(d_{3/2}^{-1}p_{1/2})$, and $(d_{3/2}^{-1}p_{3/2})$ configurations were also tried, but yielded cross sections that decreased faster with increasing E_0 than the $E1$ fit shown in Fig. 8. For $\theta = 163°$ and $E_0 = 60$ MeV, the $(f_{7/2}^{-1}g_{9/2})$ particle-hole configuration yields a maximum $M2$ cross section of 31 nb/sr which is an order of magnitude larger than for the other configurations. This corresponds to a $B(M2)\downarrow$ of $100\mu_N^2\,\text{fm}^2$. The configurations chosen for the 6.41 MeV state appears to be a combination of $M1$ and $M2$. Since our energy resolution is much broader than the average energy level spacing, it is possible that more than one state is excited.

The most outstanding similarity of all distributions in Fig. 8 is that as a group they all are best fitted by an $M2$ assignment from 50 to 75 MeV. Below 50 MeV the cross section increases for some of these states indicating a mixture of $M1$ and $M2$ transitions. Two broad unresolved groups are the 5.92-6.05 and the 7.09-7.24 MeV states. Each pair has been curve fitted and the decomposition is shown in Fig. 9 fitted by $M1$ and $M2$ transitions. The vertical extent of the bars indicates the level of uncertainty in decomposing each group into two levels. The 6.05 and 7.09 MeV states are now best fitted by an $M1$ transition. The 5.92 and 7.24 MeV transitions can be fitted by an $M2$ transition.

If the 6.05, 6.41, and 7.09 MeV states have $J^\pi = 1^+$ assignments, then the $M1$ transition strength to these states would be 0.37, 0.12, and $0.44\mu_N^2$. This sums to $0.93\mu_N^2$ and its centroid is about $E_x = 6.6$ MeV, about 4 MeV lower than the T_0+1, $M1$ strength and about half its strength.

The dominant behavior of the 6.83 and 8.23 MeV transitions from 40 to 75 MeV is $M2$. The 7.53 and 8.51 MeV transitions are also consistent with an $M2$ assignment. Since we are unable to make a meaningful cross section determination at 40 MeV for the 7.53 and 8.51, we cannot unambiguously eliminate contributions from $M1$ transitions, although it does appear, however, that such contributions may be small. The 9.85 MeV state was previously discussed.

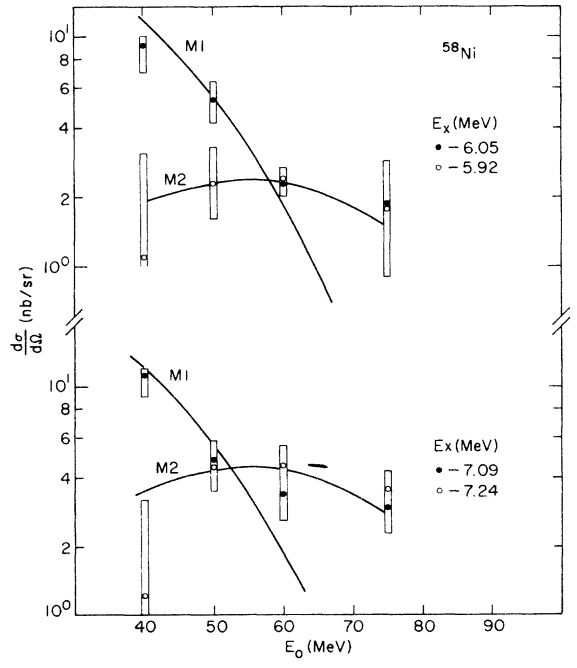

FIG. 9. Decomposition of the differential cross section at $\theta = 160°$ for the partially resolved $E_x = 5.92$ and 6.05 MeV and $E_x = 7.09$ and 7.24 MeV states as a function of E_0, the incident electron bombarding energy. The data are shown compared to $M1$ and $M2$ DWBA calculations.

Shell model calculations by Ngo-Trong and Rowe[21] predict a 2^- state at 7.77 MeV with $B(M2)\downarrow = 87\mu_N^2\,\mathrm{fm}^2$, several other weaker states between $E_x = 6$ and 10 MeV excitation, and four strong states clustered near 11.0 MeV excitation. If we assume the 5.92, 6.41, 6.83, 7.09, 7.53, 8.23, and 8.51 MeV states are excited by $M2$, the measured $M2$ strength summed over these states is about $B(M2)\downarrow = 100\mu_N^2\,\mathrm{fm}^2$, which is about 30% of the calculated $M2$ strength[21] over about the same region of excitation energy.

V. MAGNETIC DIPOLE CLOSURE SUM RULE

It is instructive to compare the measured T_0+1 strength with the closure sum rule.[22,23] This comparison is simpler and less ambiguous than comparing with the Kurath energy-weighted $M1$ sum rule[24] for nuclei in the $f_{7/2}$ shell, where the tensor corrections to the sum rule may not be negligible. We have obtained the T_0+1 closure sum-rule limit by evaluating the $M1$ operator at the photon point between the model excited state $1/\sqrt{2}\,[(f_{7/2}^{-1}f_{5/2})_p - (f_{7/2}^{-1}f_{5/2})_n]_{1^+,T_0+1}$ and the closed ^{58}Ni ground state $\{[(f_{7/2}^{8})_p(f_{7/2}^{8})_n]_{0^+,0}[(p_{3/2}^{2})_n]_{0^+,T_0}\}_{0^+,T_0}$. The $M1$ transition strength[22,23] from the isobaric analog state to the ground state is

$$B(M1)\downarrow = \frac{1}{T_0+1}\,\frac{1}{\pi}\,\frac{(l)(l+1)}{2l+1}\,[(\mu_n - \mu_p + \tfrac{1}{2})^2]\mu_N^2. \quad (1)$$

The total T_0+1, $M1$ strength for ^{58}Ni in Table II is $1.89\mu_N^2$, 39% of the limit of $4.81\mu_N^2$ obtained from Eq. (1) with $T=1$ and $l=3$. If we do not include the 9.81 MeV state, the sum reduces slightly to 33% of the $M1$ sum-rule limit. However, some realistic shell model calculations[25] predict that in the ^{58}Ni ground state the $f_{7/2}$ orbit is only 50%–70% full. Since we have computed the $M1$ sum-rule limit assuming the $f_{7/2}$ orbit is 100% full, we have in all likelihood overestimated the available $M1$ strength. The sum-rule limit is directly proportional to the percentage that the $f_{7/2}$ orbit is full. Since these shell model calculations predict the orbit to be 50% full in one case, this reduces the $M1$ sum-rule limit by a factor of 2. Therefore, the fraction of observed $M1$ strength increases from 33%–39% to 66%–78% of the available $M1$ strength. Furthermore, if in the ^{58}Ni ground state the $f_{5/2}$ orbit were partially occupied, producing a blocking effect, the sum-rule limit would decrease even more.

For the T_0, $M1$ states the $p_{3/2}$ neutrons in the ground state contribute to the closure sum rule as well as the $f_{7/2}$ shell nucleons increasing the limit to $5.59\mu_N^2$. If the 6.05, 6.41, and 7.09 MeV states have $J^\pi = 1^+$ assignments, then their summed $M1$ transition strength is about $B(M1) \simeq 0.9\mu_N^2$, which is about 16% of the calculated limit.

Limited measurements, made at 40 and 50 MeV at 180° on ^{60}Ni, are shown in Fig. 5. The 11.89 and 12.31 peaks are identified as isobaric analog $M1$ states by comparing to the known[19] 1^+ states in ^{60}Co tabulated in Table II. Possible 1^+ states at higher excitation energies are too weak to be unambiguously identified. For ^{60}Ni the sum of $T_0 + 1$, $M1$ strength in Table II is $0.90\mu_N^2$, about 28% of the closure sum-rule limit of $3.21\mu_N^2$ given in Eq. (1). For just the 11.9 and 12.3 MeV levels the sum is 22% of the limit. No multipole assignments could be made to states in ^{60}Ni below the analog states because of poor energy resolution and background. However, further measurements in the nickel and iron isotopes are planned using a higher energy resolution system to systematically study the $M1$ transitions in this mass region.

VI. CONCLUSIONS

It is clear from the energy dependence of the cross section and the comparison with the known 1^+ states in the parent nuclei ^{58,60}Co that we have identified a sizable fraction of the isobaric analog $M1$ strength in ^{58,60}Ni. It is concentrated in the lowest few $T_0 + 1$, 1^+ levels, which lie within a 1 MeV energy interval. The presence or absence of T_0, $M1$ strength was not conclusive. Clearly, higher energy resolution measurements and realistic model calculations would be very desirable in helping to understand the magnitude, fragmentation, and isospin nature of the giant $M1$ and $M2$ strength in this mass region.

ACKNOWLEDGMENTS

We are happy to acknowledge Professor H. Überall for many helpful discussions, and Dr. D. Kurath for his assistance regarding the use of $M1$ sum rules. We also would like to acknowledge Dr. S. Penner and the Linac staff at the National Bureau of Standards and Dr. T. F. Godlove and the Linac staff at the Naval Research Laboratory.

---

*On leave from the University of Rochester, New York 14627. Present address: Catholic University, Washington, D. C. 20017.

†Visitor from Naval Postgraduate School, Monterey, California 93940: Permanent address: National Bureau of Standards, Gaithersburg, Maryland 20234.

[1]T. W. Donnelly and G. E. Walker, Ann. Phys. (N.Y.) 60, 209 (1970).

[2]A. Bohr and B. R. Mottelson, *Nuclear Structure* (Benjamin, New York, 1975), Vol. II, Chap. 6.

[3]L. W. Fagg, Rev. Mod. Phys. 47, 683 (1975).

[4]R. Pitthan and T. Walcher, Phys. Lett. 36B, 563 (1971); R. J. Holt and H. E. Jackson, Phys. Rev. C 12, 56 (1975).

[5]C. D. Bowman, R. J. Baglan, B. L. Berman, and T. W. Philips, Phys. Rev. Lett. 25, 1302 (1970).

[6]R. E. Toohey and H. E. Jackson, Phys. Rev. C 6, 1440 (1972); R. J. Holt and H. E. Jackson, Phys. Rev. Lett. 36, 244 (1976).

[7]M. Obu and T. Terasawa, Prog. Theor. Phys. 43, 1231 (1970).

[8]E. R. Flynn and J. D. Garrett, Phys. Rev. Lett. 29, 1748 (1972).

[9]F. Cannata, B. A. Lamers, C. W. Lucas, A. Nagl, H. Uberall, C. Werntz, and F. J. Kelly, Can. J. Phys. 52, 1405 (1974).

[10]B. T. Chertok, C. Sheffield, J. W. Lightbody, Jr., and S. Penner, Phys. Rev. C 8, 23 (1973).

[11]P. J. Moffa and G. E. Walker, Nucl. Phys. A222, 140 (1974).

[12]P. T. Kan, G. A. Peterson, D. V. Webb, B. M. Szalata, J. W. O'Connell, S. P. Fivozinsky, J. W. Lightbody, Jr., and S. Penner, Phys. Rev. C 12, 1118 (1975).

[13]T. DeForest and J. D. Walecka, Advan. Phys. 15, 1 (1966).

[14]H. Nguyen-Ngoc and J. P. Perez-y-Jorba, Phys. Rev. 136, B1036 (1964).

[15]M. A. Duguay, C. K. Bockelman, T. H. Curtis, and R. A. Eisenstein, Phys. Rev. 163, 1259 (1967).

[16]M. J. Schneider and W. W. Daehnick, Phys. Rev. C 5, 1330 (1972); T. Caldwell, O. Hansen, and D. J. Pullen, Nucl. Phys. A202, 225 (1973).

[17]J. A. Nolen and J. P. Schiffer, Annu. Rev. Nucl. Sci. 19, 519 (1969).

[18]H. C. Lee, Chalk River Nuclear Laboratories Report No. AECL-4839 (unpublished).

[19]W. Seliger, D. Backner, H. Kelleter, and B. Schmidt, Nucl. Phys. A184, 599 (1972).

[20]A. J. F. Siegert, Phys. Rev. 52, 787 (1937).

[21]C. Ngo-Trong, Ph.D. thesis, University of Toronto, 1974 (unpublished), under D. J. Rowe.

[22]S. Yoshida and L. Zamick, Annu. Rev. Nucl. Sci. 22, 121 (1972).

[23]D. Kurath (private communication).

[24]D. Kurath, Phys. Rev. 130, 1525 (1963).

[25]G. Oberlechner and J. Richert, Nucl. Phys. A191, 577 (1972).